

Experimental Testing on an Effective Technique to Reconstruct the Far-Field Pattern of a Long Antenna from Near-Field Measurements Acquired via Spherical Spiral Scan

F. D'Agostino, F. Ferrara, C. Gennarelli*, R. Guerriero and M. Migliozi

Dipartimento di Ingegneria Industriale (D.I.In.) - University of Salerno, via Giovanni Paolo II, 84084 Fisciano (Salerno), Italy

Abstract: In this paper, the experimental validation of a fast and accurate near-field – far-field (NF–FF) transformation with spherical spiral scanning for elongated antennas is provided. Such a transformation relies on a nonredundant sampling representation of the voltage measured by the probe, obtained by using the unified theory of spiral scans for non-spherical antennas and adopting a cylinder ended in two half-spheres to model long antennas. It allows a remarkable reduction of the measurement time due to the use of continuous and synchronized movements of the positioning systems and to the reduced number of needed NF measurements. In fact, the NF data required by the classical spherical NF–FF transformation are efficiently and accurately recovered from those collected along the spiral, by using an optimal sampling interpolation expansion. Experimental results, obtained at the Antenna Characterization Lab of the University of Salerno and assessing the effectiveness of such a NF–FF transformation, are shown.

Keywords: Antenna measurements, Near-field – far-field transformation techniques, Spherical spiral scanning, Nonredundant sampling representations of electromagnetic fields.

1. INTRODUCTION

The techniques for the reconstruction of antenna far-field (FF) patterns from measurements accomplished in the near-field (NF) region have been widely investigated and employed in the last four decades [1-7], since they allow to overcome all drawbacks which make impractical the direct measurement in a conventional FF range. Moreover, they represent the most convenient choice when complete pattern and polarization measurements are required, and can be used to determine the field at the antenna surface. This information can be properly exploited for the diagnostics of faulty elements in an array or surface deformations in a reflector antenna (microwave holographic diagnostics [8]). Usually, the FF patterns are obtained from the measured NF data by using an expansion of the field of the antenna under test (AUT) in terms of modes, i.e., a complete set of solutions of the vector wave equation in the region outside the antenna. Plane, cylindrical, or spherical waves are normally employed. The type of modal expansion adopted to represent the field determines the kind of the NF scanning surface, which, therefore, will be a plane, a cylinder, or a sphere. The modal expansion coefficients, whose knowledge allows the reconstruction of the AUT far field, are then obtained by exploiting the orthogonality properties of the modes on these surfaces. The employment of NF–FF transformations using different scanning geometries is justified from the fact that

each approach has its own specific advantages, depending on the measurement requests and on the AUT characteristics. In particular, that making use of the spherical scan has attracted a considerable interest [9-21], because it allows the whole reconstruction of the AUT pattern without requiring its repositioning and avoids the errors due to the scanning surface truncation. However, this is obtained at the expense of a data processing remarkably heavier than that needed in the planar and cylindrical scanning cases.

Innovative NF–FF transformation techniques with spherical spiral scanning have been proposed in recent years [22-29]. They maintain the interesting features of those employing the spherical scanning and, what's more, reduce in a remarkable way the time required for the NF data acquisition, which, as suggested in [30], is performed on fly by exploiting continuous and synchronized movements of the positioning systems of the probe and AUT. It must be stressed that the reduction of the measurement time is a very important issue for the antenna measurement community, since such a time is nowadays very much greater than that required to evaluate the far field by means of the NF–FF transformation code. The remarkable time saving characterizing these innovative transformations is even more strengthened by the reduced number of the NF data to be collected. As a matter of fact, they are based on the nonredundant sampling representations of electromagnetic (EM) fields [31, 32] and make use of proper optimal sampling interpolation (OSI) expansions [33] to retrieve, from the nonredundant samples acquired along the spiral, the NF data required by the NF–FF transformation with spherical scanning in its original version [13] or as modified in [14, 16]. The nonredundant sampling

*Address correspondence to this author at the Dipartimento di Ingegneria Industriale (D.I.In.) - University of Salerno, via Giovanni Paolo II, 84084 Fisciano (Salerno), Italy; Tel: +39 089 964297; Fax: +39 089 968730; E-mails: cgennarelli@unisa.it, gennar@diie.unisa.it

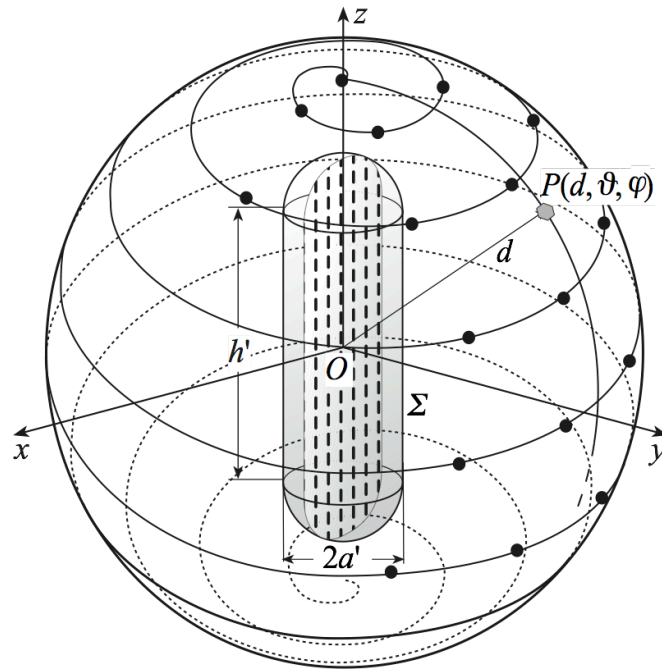


Fig. (1). Spherical spiral scanning for an elongated antenna.

representation on the sphere for the voltage measured by the probe has been obtained by choosing the spiral in such a way that it intersects any meridian at points whose spacing coincides with that needed for the interpolation and then determining a nonredundant representation on such a spiral. In a first approach, the sampling representation has been determined [22-24] by adopting a spherical source modelling, i.e., by considering the AUT as enclosed in the smallest sphere able to contain it. Then, by properly applying the unified theory of spiral scans for nonspherical antennas [25], NF-FF transformations with spherical spiral scanning for elongated or quasi-planar antennas have been developed in [26-29], thus avoiding the useless increase in the number of the NF data to be acquired, related to the use of the spherical modelling when considering these kinds of antennas. More in detail, an oblate [26, 28] and a prolate ellipsoid [26] have been employed to shape a quasi-planar and an elongated antenna, respectively. As an alternative, a quasi-planar antenna has been considered as enclosed in a surface formed by two circular bowls with the same aperture diameter but eventually different lateral bends [27, 29] and a rounded cylinder, namely, a cylinder ended in two half-spheres has been adopted for modelling an elongated AUT [27]. Generally, the use of these last modellings results to be more effective from the data reduction viewpoint with respect to the employment of the corresponding ellipsoidal ones, since they allow a better fitting of many antennas by properly setting their geometric parameters.

The goal of this paper is the experimental validation of the NF-FF transformation with spherical spiral scan for long antennas [27] based on the rounded cylinder modelling (see Fig. 1). The effectiveness of that for quasi-planar antennas using the two-bowls modelling has been already assessed in [29]. Also in such a case, the testing has been carried out by means of the spherical NF facility available in the anechoic chamber of the Antenna Characterization Lab of the Univer-

sity of Salerno and has wholly confirmed the effectiveness of this innovative transformation, which allows a remarkable time saving without losing the accuracy of the classical spherical one.

2. NONREDUNDANT SAMPLING REPRESENTATION OF THE PROBE VOLTAGE ON A SPHERE

Let us consider an elongated antenna and a nondirective probe scanning a proper spiral, which wraps a spherical surface of radius d in the antenna NF region, and adopt the spherical coordinate system (r, ϑ, φ) for denoting an observation point P (Fig. 1). It has been shown [34] that the voltage V measured by such a kind of probe has the same effective spatial bandwidth of the AUT field and, accordingly, the nonredundant sampling representations of EM fields [31] can be applied to it. Therefore, when dealing with the representation on a curve C , it is convenient to use a proper analytical parameterization $\underline{r} = \underline{r}(\eta)$ for describing C and to introduce the “reduced voltage”

$$\tilde{V}(\eta) = V(\eta) e^{j\psi(\eta)} \quad (1)$$

where V is the voltage V_1 or V_2 measured by the probe or by the rotated probe and $\psi(\eta)$ is a proper phase function. As shown in [31], $\underline{r}(\eta)$ and $\psi(\eta)$ are related to the rotational surface Σ bounding the convex domain adopted to model the AUT. The choice of a modelling which fits the geometry of the AUT well is mandatory for minimizing the number of required samples. Since the considered AUT is long, it is convenient to choose the surface Σ enclosing it coincident with a rounded cylinder, namely, a cylinder of height h' ended in two half-spheres of radius a' (see Figs. 1 and 2). The error, occurring when $\tilde{V}(\eta)$ is approximated by a band-limited function, exhibits a step-like behaviour becoming

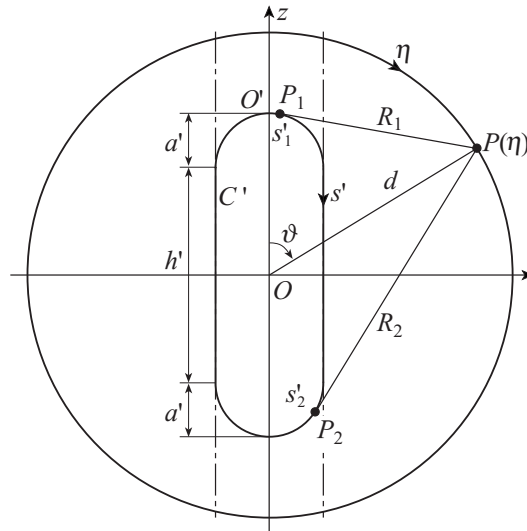


Fig. (2). Relevant to the rounded cylinder modelling.

negligible as the bandwidth exceeds a critical value W_η [31] and can be effectively controlled by choosing the bandwidth of the approximating function equal to $\chi'W_\eta$, χ' being an enlargement bandwidth factor, which is slightly greater than unity for electrically large antennas.

According to the unified theory of spiral scans for non-spherical antennas [25], the OSI expansion for the voltage reconstruction on a sphere from a nonredundant number of its samples acquired by the probe along a proper spiral can be derived by choosing the spiral in such a way that it intersects any meridian at points whose spacing coincides with that needed for the interpolation and then determining a non-redundant representation on such a spiral. Because of the choice of a rounded cylinder as modelling, the bandwidth W_η , the parameterization η relevant to a meridian and the corresponding phase function ψ are [27, 31]:

$$W_\eta = \beta \ell' / 2\pi \tag{2}$$

$$\eta = (\pi / \ell') [R_1 - R_2 + s'_1 + s'_2] \tag{3}$$

$$\psi = (\beta / 2) [R_1 + R_2 + s'_1 - s'_2] \tag{4}$$

where β is the wavenumber, $\ell' = 2(h' + \pi a')$ is the length of the intersection curve C' between the meridian plane through the observation point P and Σ , $R_{1,2}$ are the distances from P to the two tangency points $P_{1,2}$ between the cone of vertex at P and C' , and $s'_{1,2}$ are their curvilinear abscissae (see Fig. 2). The expressions of $R_{1,2}$ and $s'_{1,2}$ change de-

pending on the location of the points $P_{1,2}$ [27] and are reported in Appendix A for reader's convenience.

As shown in [25], the spiral can be obtained by projecting on the scanning sphere, via the curves at $\eta = \text{const}$ [27], a proper spiral wrapping Σ whose pitch is equal to the sample spacing $\Delta\eta = 2\pi / (2N'' + 1)$ required for interpolating the voltage along a meridian. In this last relation, $N'' = \text{Int}(\chi N') + 1$, where $N' = \text{Int}(\chi'W_\eta) + 1$, $\text{Int}(x)$ is the integer part of x , and $\chi > 1$ is an oversampling factor needed to control the truncation error [31, 33]. Accordingly, the parametric equations of the spiral are [25, 27]:

$$\begin{cases} x = d \sin \theta(\eta) \cos \phi \\ y = d \sin \theta(\eta) \sin \phi \\ z = d \cos \theta(\eta) \end{cases} \tag{5}$$

wherein ϕ is the angular parameter describing the spiral and $\eta = k\phi$. The parameter k is such that the spiral step, determined by two consecutive intersections with a meridian, coincides with the sample spacing $\Delta\eta$. Accordingly, since $\Delta\eta = 2\pi k$, it follows that $k = 1 / (2N'' + 1)$. It must be stressed that the spiral angle θ , unlike the zenithal angle ϑ , can assume negative values.

The way for determining a nonredundant representation on the spiral is again traced by the unified theory of spiral scanings for nonspherical antennas. Accordingly, the optimal parameter ξ to describe the spiral is equal to β / W_ξ times the arclength of the projecting point on the spiral which wraps the modelling surface Σ and the corresponding phase function γ coincides with that ψ relevant to a meridian.

The bandwidth W_ξ is chosen equal to β/π times the length of the spiral wrapping Σ from pole to pole [25, 27], so that ξ covers a 2π range when a point moving on the scanning spiral encircles the AUT once. It must be stressed that, in such a way, the spiral, γ and ξ coincide with those relevant to the spherical modelling when the surface Σ reduces to a sphere [25].

By taking into account the above results, the voltage at P on the meridian at φ can be reconstructed via the following OSI formula [27]:

$$V(\eta(\vartheta), \varphi) = e^{-j\psi(\eta)} \sum_{n=n_0-q+1}^{n_0+q} \tilde{V}(\eta_n) G(\eta, \eta_n, \bar{\eta}, N, N'') \quad (6)$$

wherein $\tilde{V}(\eta_n)$ are the intermediate reduced samples, namely, the reduced voltage values at the intersection points between the meridian passing through P and the spiral, $2q$ is the number of the retained samples, $n_0 = \text{Int}[(\eta - \eta_0)/\Delta\eta]$, $\bar{\eta} = q\Delta\eta$, $N = N'' - N'$, and

$$\eta_n = \eta_n(\varphi) = k\varphi + n\Delta\eta = \eta_0 + n\Delta\eta \quad (7)$$

Moreover,

$$G(\eta, \eta_n, \bar{\eta}, N, N'') = D_{N''}(\eta - \eta_n) \Omega_N(\eta - \eta_n, \bar{\eta}) \quad (8)$$

is the product of the Dirichlet and Tschebyscheff sampling functions [31, 33]:

$$D_{N''}(\eta) = \frac{\sin((2N''+1)\eta/2)}{(2N''+1) \sin(\eta/2)} \quad (9)$$

$$\Omega_N(\eta, \bar{\eta}) = \frac{T_N[-1 + 2(\cos(\eta/2)/\cos(\bar{\eta}/2))^2]}{T_N[-1 + 2/\cos^2(\bar{\eta}/2)]} \quad (10)$$

wherein $T_N(\eta)$ is the Tschebyscheff polynomial of degree N .

A similar OSI expansion along the spiral [27] allows to retrieve the intermediate reduced samples $\tilde{V}(\eta_n)$:

$$\tilde{V}(\eta_n) = \tilde{V}(\xi(\eta_n)) = \sum_{m=m_0-p+1}^{m_0+p} \tilde{V}(\xi_m) G(\xi, \xi_m, \bar{\xi}, M, M'') \quad (11)$$

where $2p$ is the number of the retained samples, $m_0 = \text{Int}[\xi/\Delta\xi]$, $\bar{\xi} = p\Delta\xi$, $M = M'' - M'$, and

$$\xi_m = m\Delta\xi = 2\pi m/(2M''+1) \quad (12)$$

with $M'' = \text{Int}(\chi M') + 1$ and $M' = \text{Int}(\chi' W_\xi) + 1$.

The two-dimensional OSI expansion to reconstruct the voltage at any point on the sphere is then obtained by matching the one-dimensional ones (6) and (11), thus getting:

$$V(\eta(\vartheta), \varphi) = e^{-j\psi(\eta)} \sum_{n=n_0-q+1}^{n_0+q} \left[G(\eta, \eta_n, \bar{\eta}, N, N'') \cdot \sum_{m=m_0-p+1}^{m_0+p} \tilde{V}(\xi_m) G(\xi, \xi_m, \bar{\xi}, M, M'') \right] \quad (13)$$

Such an expansion allows the accurate reconstruction of the voltages V_1 and V_2 , which would be measured by the probe and rotated probe at the points required by the spherical NF-FF transformation in its classical version [13] or as modified in [16].

3. EXPERIMENTAL ASSESSMENT

Some experimental tests assessing the effectiveness of the described NF-FF transformation with spherical spiral scanning for long antennas are shown in this section. They have been accomplished in the anechoic chamber of the Antenna Characterization Lab of the University of Salerno, wherein a roll (φ axis) over azimuth (ϑ axis) spherical NF facility is available. The chamber is $8\text{m} \times 5\text{m} \times 4\text{m}$ sized and is covered with pyramidal absorbers which guarantee a wall reflectivity less than -40 dB. It is equipped with a vertical scanner and some rotating tables supplied by MI Technologies, which can be properly arranged to perform NF measurements with plane-polar, planar spiral, cylindrical, and helicoidal scannings, besides those with spherical and spherical spiral scannings. Direct FF measurements and radar cross section (RCS) measurements of small targets are also possible. The amplitude and phase measurements are carried out by means of a vectorial network analyzer Anritsu 37247C, which is characterized by wide dynamic range, high sensitivity and linearity in the frequency range from 40 MHz to 20 GHz. Both the rotating tables employed in the roll over azimuth spherical NF facility assure an angular precision of $\pm 0.05^\circ$.

The experimental results reported in the following refer to the field radiated at 10.4 GHz by a X-band resonant slotted waveguide array made by PROCOM A/S, realized by cutting 12 round-ended slots on both the broad walls of a WR90 rectangular waveguide and soldering two cylinders on its narrow walls (see Fig. 3). Such an antenna has been modelled by a rounded cylinder with $h' = 28.28$ cm, $a' = 2.60$ cm and mounted in such a way that the broad walls are parallel to the plane $y = 0$ and its axis is coincident with the z one. The probe output voltages have been acquired by an open-ended WR90 rectangular waveguide on a spiral wrapping a sphere with radius $d = 45.2$ cm.

In order to assess the effectiveness of the two-dimensional OSI algorithm (13), the amplitude and phase of the reconstructed voltage V_1 relevant to the meridian at $\varphi = 0^\circ$ are compared in Figs. (4 and 5), respectively, with those directly measured on the same meridian. The corresponding comparisons relevant to the meridian at $\varphi = 90^\circ$ are shown in Figs. (6 and 7). As regards the values of the OSI algorithm parameters, χ' has been chosen equal to 1.30 in order to

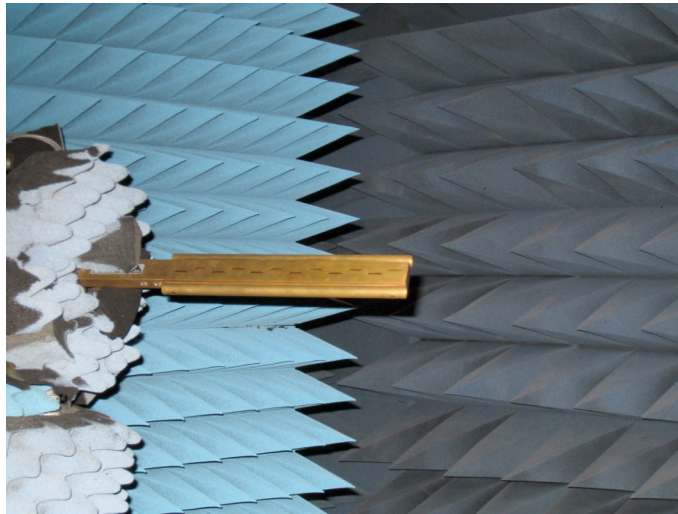


Fig. (3). Photo of the X-band resonant slotted waveguide array.

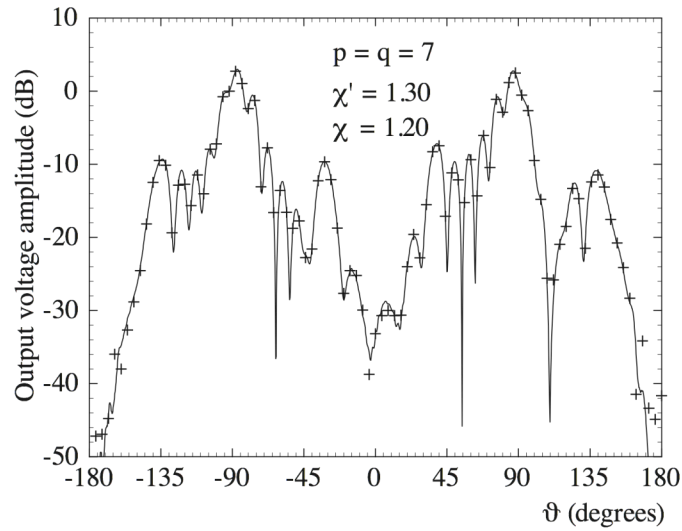


Fig. (4). Amplitude of V_1 on the meridian at $\varphi = 0^\circ$. Solid line: measured. Crosses: recovered from NF data acquired *via* the spherical spiral scanning.

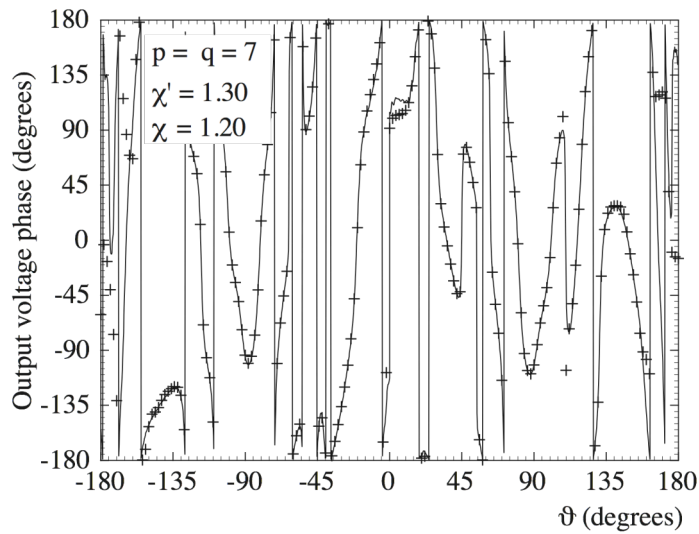


Fig. (5). Phase of V_1 on the meridian at $\varphi = 0^\circ$. Solid line: measured. Crosses: recovered from NF data acquired *via* the spherical spiral scanning.

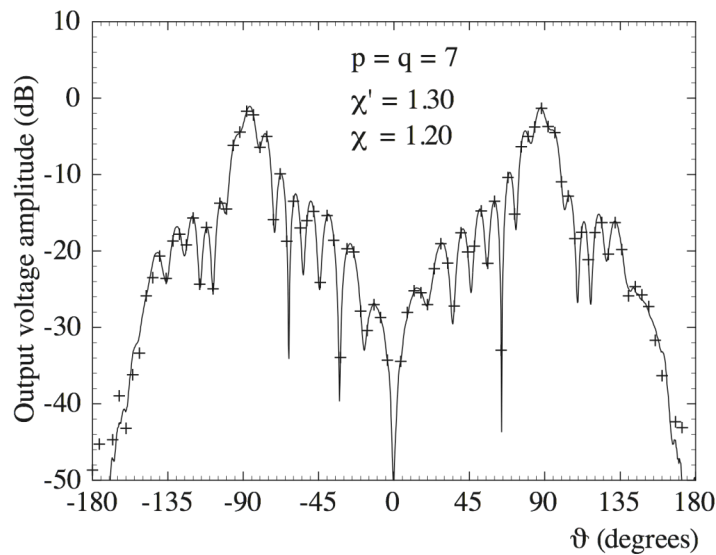


Fig. (6). Amplitude of V_1 on the meridian at $\varphi = 90^\circ$. Solid line: measured. Crosses: recovered from NF data acquired *via* the spherical spiral scanning.

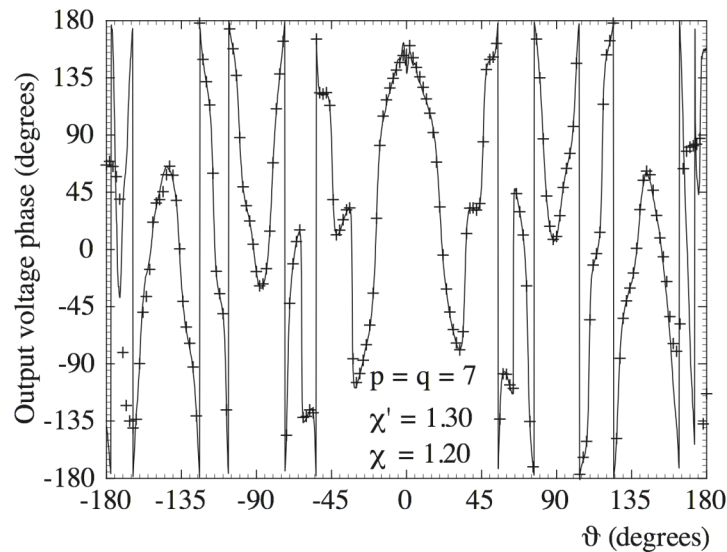


Fig. (7). Phase of V_1 on the meridian at $\varphi = 90^\circ$. Solid line: measured. Crosses: recovered from NF data acquired *via* the spherical spiral scanning.

make negligible the aliasing error with respect to the measurement one [35], whereas $\chi = 1.20$ and $p = q = 7$ have been employed for neglecting the truncation error [27]. A good agreement between the retrieved voltage (crosses) and that directly acquired (solid line) results save for the zones characterized by a very low level, wherein the error is due to the noise and the residual reflections from the anechoic chamber walls. Note that an enlargement bandwidth factor χ' such that the spacing among the samples is reduced exactly by a factor 5 has been adopted in the zones of the spiral determined by the 20 samples around each pole.

The overall effectiveness of this NF–FF transformation technique is assessed by comparing the FF patterns in the principal planes E and H recovered from the NF data col-

lected along the spiral (Figs. 8 and 9) with those (references) obtained from the NF data directly acquired on the classical spherical grid. Note that the software package MI-3000, implementing the standard spherical NF–FF transformation [13], has been used to reconstruct the FF patterns in both the cases. At last, the FF pattern reconstruction in the cut plane at $\varphi = 90^\circ$ is shown in Fig. (10). In this last figure, as well as in Fig. (9), it is plotted also the reconstruction error in order to better appreciate its levels. All reconstructions are very accurate, thus validating also from the experimental point of view the effectiveness of the described technique.

It must be stressed that the number of employed samples is 1 024 (including the 160 “extra samples” at reduced spacing) and, therefore, significantly less than those (5 100 and 3 622) which would be respectively required by the MI soft-

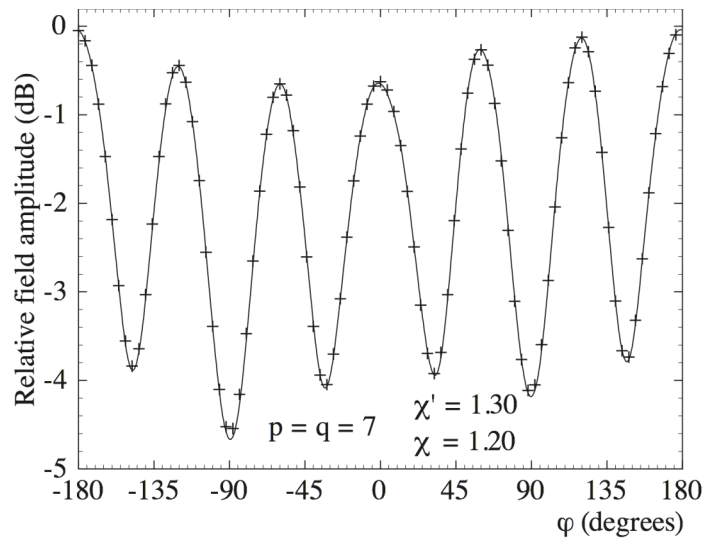


Fig. (8). E-plane pattern. Solid line: reference. Crosses: recovered from NF data acquired via the spherical spiral scanning.

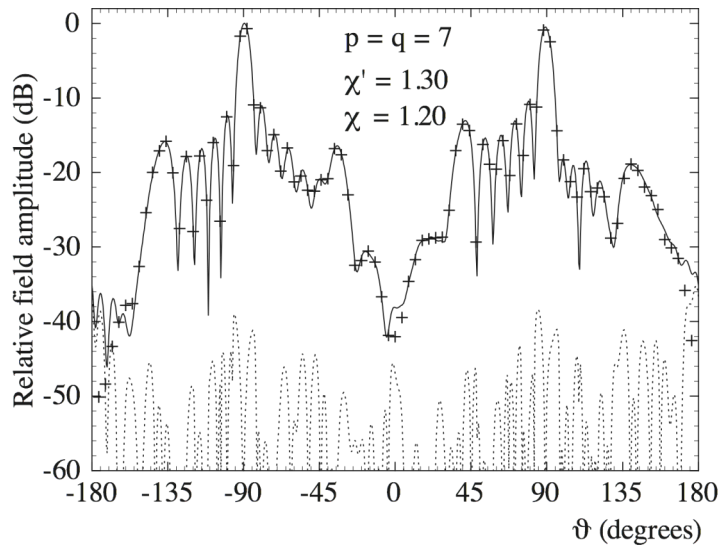


Fig. (9). H-plane pattern. Solid line: reference. Crosses: recovered from NF data acquired via the spherical spiral scan. Dashed line: reconstruction error.

ware package implementing the classical spherical NF–FF transformation [13] and by the NF–FF transformation with spherical spiral scan [23, 24] based on the spherical AUT modelling. It is worth noting that these reduction percentages are much greater than the corresponding ones obtained in [29], wherein the two-bowls modelling was adopted to shape a quasi-planar antenna. This result does not depend on the particular antennas considered in these two papers, but is a general validity result: the time saving obtainable by using the appropriate spiral scanning technique when considering long antennas is usually remarkably greater than that in the quasi-planar antennas case. In fact, the number of spiral turns is related to the length of the curve C' , whereas the average number of samples on a turn depends on the maximum transverse radius of Σ .

4. CONCLUSIONS

The innovative NF–FF transformation with spherical spiral scanning for elongated antennas, based on the rounded

cylinder modelling, has been experimentally tested in this paper. A very good agreement has been found, both in the near-field and in the far-field reconstructions, thus experimentally confirming the effectiveness and reliability of such a transformation technique, which is even more effective from the data reduction and measurement time saving viewpoints than that for quasi-planar antennas [29].

APPENDIX A. EXPLICIT EXPRESSIONS OF $R_{1,2}$ AND $s'_{1,2}$

In this appendix, the explicit expressions of the parameters involved in the nonredundant sampling representation relevant to a meridian are reported. As shown in [27], the expressions of the distances $R_{1,2}$ and arclength coordinates

$s'_{1,2}$ change depending on the position of the observation point P and three cases (see Fig. 2) must be considered when ϑ varies in the range $[0, \pi]$.

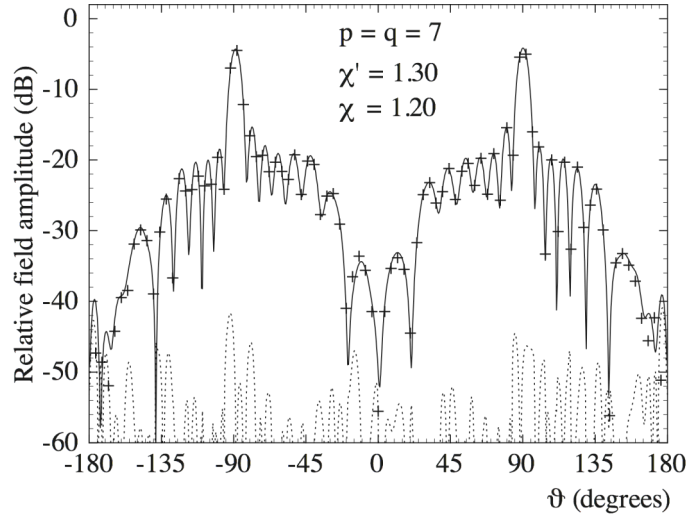


Fig. (10). FF pattern in the cut plane at $\varphi = 90^\circ$. Solid line: reference. Crosses: recovered from NF data acquired *via* the spherical spiral scanning. Dashed line: reconstruction error.

For $0 \leq \vartheta \leq \sin^{-1}(a'/d)$, it results:

$$R_1 = \sqrt{(d \sin \vartheta)^2 + (d \cos \vartheta - h'/2)^2} - a'^2 \quad (\text{A1})$$

$$s'_1 = a' \sin^{-1} \left(\frac{a' d \sin \vartheta + R_1 (h'/2 - d \cos \vartheta)}{R_1^2 + a'^2} \right) \quad (\text{A2})$$

$$R_2 = R_1; \quad s'_2 = a' \sin^{-1} \left(\frac{a' d \sin \vartheta - R_2 (h'/2 - d \cos \vartheta)}{R_2^2 + a'^2} \right) \quad (\text{A3})$$

For $\sin^{-1}(a'/d) < \vartheta \leq \pi - \sin^{-1}(a'/d)$, R_1 and s'_1 are again given by (A1) and (A2), whereas it results:

$$R_2 = \sqrt{(d \sin \vartheta)^2 + (d \cos \vartheta + h'/2)^2} - a'^2 \quad (\text{A4})$$

$$s'_2 = h' + a' \left[\pi - \sin^{-1} \left(\frac{a' d \sin \vartheta + R_2 (h'/2 + d \cos \vartheta)}{R_2^2 + a'^2} \right) \right] \quad (\text{A5})$$

At last for $\pi - \sin^{-1}(a'/d) < \vartheta \leq \pi$, R_2 and s'_2 are again given by (A4) and (A5), whereas:

$$R_1 = \sqrt{(d \sin \vartheta)^2 + (d \cos \vartheta + h'/2)^2} - a'^2 \quad (\text{A6})$$

$$s'_1 = h' + a' \left[\frac{\pi}{2} - \sin^{-1} \left(\frac{R_1 d \sin \vartheta + a' (h'/2 + d \cos \vartheta)}{R_1^2 + a'^2} \right) \right] \quad (\text{A7})$$

CONFLICT OF INTEREST

The authors confirm that this article content has no conflicts of interest.

ACKNOWLEDGMENTS

Declared none.

REFERENCES

- [1] R. C. Johnson, H. A. Ecker, and J. S. Hollis, "Determination of far-field antenna patterns from near-field measurements," *Proc. of IEEE*, vol. 61, pp. 1668–1694, December 1973.
- [2] J. Appel-Hansen, J.D. Dyson, E.S. Gillespie, and T.G. Hickman, "Antenna measurements," chapter 8 in *The handbook of antenna design*, A.W. Rudge, K. Milne, A.D. Olver, and P. Knight, Eds., London, UK, Peter Peregrinus, 1986.
- [3] A.D. Yaghjian, "An overview of near-field antenna measurements," *IEEE Trans. Antennas Propag.*, vol. AP-34, pp. 30-45, January 1986.
- [4] E. S. Gillespie, Ed., "Special issue on near-field scanning techniques," *IEEE Trans. Antennas Propag.*, vol. AP-36, pp. 727-901, June 1988.
- [5] M.H. Francis and R.W. Wittmann, "Near-field scanning measurements: theory and practice," chapter 19 in *Modern antenna handbook*, C.A. Balanis, Ed., Hoboken, NJ, John Wiley & Sons, Inc., 2008.
- [6] C. Gennarelli, A. Capozzoli, L. Foged, J. Fordham, and D.J. van Rensburg, Eds., "Special issue on recent advances in near-field to far-field transformation techniques," *Int. J. Antennas Propag.*, vol. 2012.
- [7] M.H. Francis, Ed., *IEEE Recommended practice for near-field antenna measurements*, IEEE Standard 1720-2012.
- [8] R.G. Yaccarino, Y. Rahmat Samii, and L.I. Williams, "The bi-polar planar near-field measurement technique, Part II: near-field to far-field transformation and holographic imaging methods," *IEEE Trans. Antennas Propag.*, vol. 42, pp. 196-204, February 1994.
- [9] P.F. Wacker, "Non-planar near-field measurements: spherical scanning," NBSIR 75-809, Boulder, CO, 1975.
- [10] F.H. Larsen, "Probe correction of spherical near-field measurements," *Electron. Lett.*, vol. 13, pp. 393–395, July 1977.
- [11] A.D. Yaghjian and R.C. Wittmann, "The receiving antenna as a linear differential operator: application to spherical near-field measurements," *IEEE Trans. Antennas Propag.*, vol. AP-33, pp. 1175-1185, November 1985.
- [12] J.E. Hansen and F. Jensen, "Spherical near-field scanning at the technical university of Denmark," *IEEE Trans. Antennas Propag.*, vol. AP-36, pp. 734-739, June 1988.
- [13] J. Hald, J.E. Hansen, F. Jensen, and F.H. Larsen, *Spherical near-field antenna measurements*, J.E. Hansen, Ed., IEE Electromagnetic Waves Series, Peter Peregrinus, London, UK, 1998.
- [14] O.M. Bucci, F. D'Agostino, C. Gennarelli, G. Riccio, and C. Savarese, "Data reduction in the NF–FF transformation technique with spherical scanning," *J. Electromagn. Waves Appl.*, vol. 15, no. 6, pp. 755-775, 2001.

- [15] T. Laitinen, S. Pivnenko, J. M. Nielsen, and O. Breinbjerg, "Theory and practice of the FFT/matrix inversion technique for probe-corrected spherical near-field antenna measurements with high-order probes," *IEEE Trans. Antennas Propag.*, vol. 58, pp. 2623–2631, August 2010.
- [16] F. D'Agostino, F. Ferrara, C. Gennarelli, R. Guerriero, and M. Migliozi, "Effective antenna modellings for NF – FF transformations with spherical scanning using the minimum number of data," *Int. J. Antennas Propag.*, vol. ID 936781, p. 11, 2011.
- [17] T.B. Hansen, "Spherical near-field scanning with higher-order probes," *IEEE Trans. Antennas Propag.*, vol. 59, pp. 4049–4059, 2011.
- [18] T.B. Hansen, "Numerical investigation of the system-matrix method for higher-order probe correction in spherical near-field antenna measurements," *Int. J. Antennas Propag.*, vol. ID 493705, p. 8, 2012.
- [19] M.A. Qureshi, C.H. Schmidt, and T.F. Eibert, "Adaptive sampling in spherical and cylindrical near-field antenna measurements," *IEEE Antennas Propag. Magaz.*, vol. 55, pp. 243-249, 2013.
- [20] F. D'Agostino, F. Ferrara, C. Gennarelli, R. Guerriero, and M. Migliozi, "Non-redundant spherical NF – FF transformations using ellipsoidal antenna modeling: experimental assessments," *IEEE Antennas Propag. Magaz.*, vol. 55, pp. 166-175, 2013.
- [21] F. D'Agostino, F. Ferrara, C. Gennarelli, R. Guerriero, and M. Migliozi, "Experimental testing of nonredundant near-field to far-field transformations with spherical scanning using flexible modellings for nonvolumetrical antennas," *Int. J. Antennas Propag.*, vol. ID 517934, p. 10, 2013.
- [22] O.M. Bucci, F. D'Agostino, C. Gennarelli, G. Riccio, and C. Savarese, "NF-FF transformation with spherical spiral scanning," *IEEE Antennas Wireless Propag. Lett.*, vol. 2, pp. 263-266, 2003.
- [23] F. D'Agostino, C. Gennarelli, G. Riccio, and C. Savarese, "Theoretical foundations of near-field-far-field transformations with spiral scannings," *Prog. Electromagn. Res.*, vol. PIER 61, pp.193-214, 2006.
- [24] F. D'Agostino, F. Ferrara, J.A. Fordham, C. Gennarelli, R. Guerriero, and M. Migliozi, "An experimental validation of the near-field - far-field transformation with spherical spiral scan," *IEEE Antennas Propag. Magaz.*, vol. 55, pp. 228-235, June 2013.
- [25] F. D'Agostino, F. Ferrara, C. Gennarelli, R. Guerriero, and M. Migliozi, "The unified theory of near-field – far-field transformations with spiral scannings for nonspherical antennas," *Prog. Electromagn. Res. B*, vol. 14, pp. 449-477, 2009.
- [26] F. D'Agostino, F. Ferrara, C. Gennarelli, R. Guerriero, M. Migliozi, and G. Riccio, "A nonredundant near-field to far-field transformation with spherical spiral scanning for nonspherical antennas," *The Open Electric. Electron. Eng. J.*, vol. 3, pp. 4-11, 2009.
- [27] F. D'Agostino, F. Ferrara, C. Gennarelli, R. Guerriero, and M. Migliozi, "Far-field reconstruction from a minimum number of spherical spiral data using effective antenna modellings," *Prog. Electromagn. Res. B*, vol. 37, pp. 43-58, 2012.
- [28] F. D'Agostino, F. Ferrara, C. Gennarelli, R. Guerriero, and M. Migliozi, "Experimental assessment of an effective near-field - far-field transformation with spherical spiral scanning for quasi-planar antennas," *IEEE Antennas Wireless Propag. Lett.*, vol. 12, pp. 670-673, 2013.
- [29] F. D'Agostino, F. Ferrara, C. Gennarelli, R. Guerriero, and M. Migliozi, "Far-field reconstruction from near-field data acquired via a fast spherical spiral scan: experimental evidences," *Prog. Electromagn. Res.*, vol. 140, pp. 719-732, 2013.
- [30] R.G. Yaccarino, L.I. Williams, and Y. Rahmat-Samii, "Linear spiral sampling for the bipolar planar antenna measurement technique," *IEEE Trans. Antennas Propag.*, vol. AP-44, pp. 1049-1051, July 1996.
- [31] O.M. Bucci, C. Gennarelli, and C. Savarese, "Representation of electromagnetic fields over arbitrary surfaces by a finite and nonredundant number of samples," *IEEE Trans. Antennas Propag.*, vol. 46, pp. 351-359, March 1998.
- [32] O.M. Bucci and C. Gennarelli, "Application of nonredundant sampling representations of electromagnetic fields to NF-FF transformation techniques," *Int. J. Antennas Propag.*, vol. ID 319856, p. 14, 2012.
- [33] O.M. Bucci, C. Gennarelli and C. Savarese, "Optimal interpolation of radiated fields over a sphere," *IEEE Trans. Antennas Propag.*, vol. AP-39, pp. 1633-1643, November 1991.
- [34] O.M. Bucci, G. D'Elia, and M.D. Migliore, "Advanced field interpolation from plane-polar samples: experimental verification," *IEEE Trans. Antennas Propag.*, vol. 46, pp. 204-210, February 1998.
- [35] C. Gennarelli, G. Riccio, V. Speranza, and C. Savarese, "Fast and accurate interpolation of radiated fields over a cylinder," *Prog. Electromagn. Res.*, vol. 8, pp. 349-375, 1994.

Received: October 09, 2013

Revised: December 22, 2013

Accepted: December 28, 2013

© D'Agostino *et al.*; Licensee Bentham Open.

This is an open access article licensed under the terms of the Creative Commons Attribution Non-Commercial License (<http://creativecommons.org/licenses/by-nc/3.0/>) which permits unrestricted, non-commercial use, distribution and reproduction in any medium, provided the work is properly cited.